A transient and non-unit-based protection technique for DC grids based on the rate-of-change (R-o-C) of the fault induced travelling wave components

Ikhide, M, Tennakoon, S, Ha, H, Griffiths, A, Subramanian, S & Adamczyk, A

DOI 10.1016/j.segan.2019.100195
ISSN 2352-4677

Publisher: Elsevier

A transient and non-unit-based protection technique for DC grids based on the rate-of-change (*R-o-C*) of the fault induced travelling wave components

BY

(1) Monday Ikhide (Corresponding Author)

Faculty of Engineering, Environment and Computing, Coventry University, Priority Street,

CV1 5FB, UK; email: monday.ikhide@coventry.ac.uk

(2)Sarath. B. Tennakoon

Department of Electrical Engineering, Staffordshire University, College Road, Stoke-on-Trent, ST4 2ED, UK; *email: s.b.tennakoon@staffs.ac.uk*

(3) Hengxu Ha

G.E Grid Solutions, Redhill Business Park, Stafford, ST16 1WT, UK

Email: *hengxu.ha@ge.com*

(4)Alison. L. Griffiths

Department of Electrical Engineering, Staffordshire University, College Road, Stoke-on-Trent, ST4 2ED, UK; *Email: a.l.Griffiths@staffs.ac.uk*

(5) Sankara Subramanian

Grid Engineering and innovation consultants, Stafford. ST17 4TR. UK

sujasank2003@yahoo.co.uk

(6) Andrzej J. Adamczyk,

G.E Grid Solutions, Redhill Business Park, Stafford, ST16 1WT, UK

Email: *andrzej.adamczyk@ge.com*

A transient and non-unit-based protection technique for DC grids based on the rate-of-change (*R-o-C*) of the fault induced travelling wave components

This paper presents a transient and non-unit-based protection scheme for consideration in DC grids of the future. The technique utilises the rate-of-change (*R-o-C*) of the associated travelling wave components following the occurrence of a fault to determine whether the fault is internal or external. For an internal fault, the product of the magnitude of the *R-o-C* of the fault induced voltage and current travelling wave following fault inception must exceed a predetermined setting, otherwise the fault is external. The DC inductor located at the cable ends provides attenuation for the high frequency contents resulting from an external fault. The ratio between the forward voltage travelling waves and the backward voltage travelling wave provides directional discrimination. This ratio is less than unity for a forward directional fault and greater than unity for reverse directional faults. The protection algorithm has been validated using PSCAD/EMTDC simulations based on full scale modular multilevel converter (MMC) - based HVDC grid. The simulation results presented, including the performances indices compared to existing and proposed methods available in literature shows the suitability and reliability of the proposed technique in distinguishing between internal and external faults. Key advantages of the proposed technique is that it simple, easily implemented, and does not rely on complex signal processing technique; and therefore it can easily be implemented to provide autonomous tripping for all relays located on the DC grid.

Keywords: DC grid protection; internal and external fault; transient based protection; fault induced travelling wave; rate-of-change (*R-o-C*) of travelling wave.

1.0 Introduction

Fault vulnerability and protection issues are major challenges in realising voltage source converter (VSC) - based multi-terminal DC grids [1-4]. Existing protection techniques for two terminal High voltage DC (HVDC) transmission systems utilising AC side circuit breakers (Figure 1.1) are not suitable for the primary protection of DC grids since it will require the de - energisation of the whole grid thereby bringing the entire grid and other sub-grids to a standstill [1,2]. Studies have also shown that transient based protection algorithms are most suitable for DC grids if the protection scheme must be dependable and reliable. In all the travelling wave-based protection (*TWBP*) principles presents the best solution since it utilises the higher frequency contents of the fault induced components, hence making it a reliable and one of fastest means of protection in power systems. Generally, the main fault characteristics are embedded in the travelling wave components.

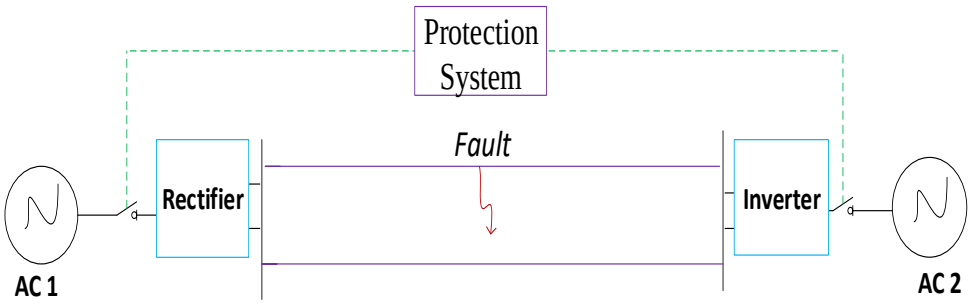

Fig. 1.1 Existing protection scheme for two terminal HVDC systems **[1]**

Several TWBP principles have been developed and proposed for power transmission systems, such as those proposed for DC grids **[3-12],** those developed for AC power transmission systems **[13-23]** and **those** proposed for two-terminal HVDC systems **[24 - 27]**. Generally, *TWBP* techniques relying on multiple reflections between the fault and the local relay terminals would results in delay. Furthermore, the travelling wave components could decay and therefore resulting in an inability to detect it at the relay terminal. This is an undesirable condition for such a scenario for the relay. In the same way, *TWBP* principle relying on communication between the local and remote end relays would also results in communication delay noting that the wave propagation delay time may be more than the time required to detect, discriminate and clear the fault. Those relying on complex DSP techniques will involve computational burden and

incur delay. In all, the trends and breakthrough as well recent advances made in the development of DC grids, such as the development of prototypes HVDC breakers [28, 29], still create opportunities for further research in DC grid protection.

The study reported in this paper utilises the rate-of-change (*R-o-C*) of the associated travelling wave components following the occurrence of a fault to determine whether a fault has occurred on a particular section or branch of the grid. For an internal fault, the product of the magnitude of the *R-o-C* of the fault induced voltage and current travelling wave following fault inception must exceed a predetermined threshold, otherwise the fault is external. The DC inductor located at the cable ends provides attenuation for the high frequency contents resulting from an external fault. The ratio between the forward voltage/current travelling waves to the backward voltage/current travelling wave provides directional discrimination. This ratio is less than unity for a forward directional fault and greater than unity for reverse directional faults. The protection algorithm has been validated using PSCAD/EMTDC simulations based on full scale modular multilevel converter (MMC) - based HVDC grid. The simulation results presented, including the performances indices presented, compared to existing and proposed methods available in literature shows the suitability and reliability of the proposed technique in distinguishing between internal and external faults.

The rest of the paper is structured as follows. In section two (2), the TWBP principle is presented, and thereafter the proposed protection algorithm presented in section three (3). The simulation studies carried out to validate the proposed protection principle are presented in four (4), whilst the complete protection scheme including the sensitivity analysis are presented in section five (5). Section six (6) concludes the paper, with some proposals and recommendations for future research direction.

2.0 Travelling wave-based protection principle

In general, the occurrence of a fault on a transmission line will result in a voltage collapse and initiate a travelling wave [15 - 19], as shown in Figure 2.1

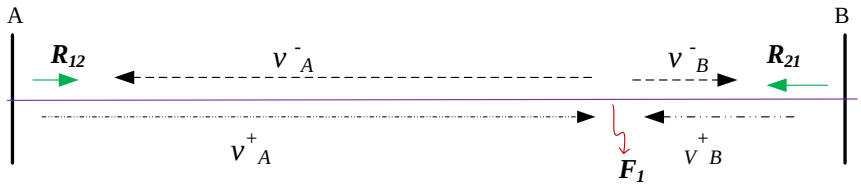

Fig. 2.1 Travelling Wave on Transmission Lines

v^+_A and v^-_A are the forward and backward travelling wave with respect to the relay A

v^+_B and v^-_B are the forward and backward travelling wave with respect to the relay B

The term forward or backward are arbitrary and depends on the assumed reference direction of current flow in the relay. Those waves travelling from the bus bar into the line are regarded as forward travelling wave (*FTW*); whilst those travelling from the line into the bus are regarded as backward travelling wave (*BTW*). Generally, v^+_A and v^-_A are also accompanied by a forward and backward current travelling wave, i^+_A and i^-_A respectively (not shown in the diagram).

The current associated with the forward travelling wave has positive polarity whilst that associated with the backward travelling wave has negative polarity. From Figure 2.1 and with R_{12} as a reference relay, the following equations can be defined.

$$\Delta v_{dc} = v^+_A(t) + v^-_A(t) \qquad (2.1)$$

$$\Delta i_{dc} = i^+_A(t) + i^-_A(t) \qquad (2.2)$$

The voltage and current travelling wave are related by the surge impedance of the line, Z_c ; thus

$$i^+ = \frac{v^+_A}{Z_c} \qquad (2.3)$$

$$i^- = -\frac{v^-_A}{Z_c} \qquad (2.4)$$

Δv_{DC} and Δi_{DC} are the superimposed components of the voltages and currents following an abrupt injection on the line. Under steady state conditions, Δv_{DC} and Δi_{DC} are ideally zero and no travelling wave is present. Combining Equations (2.1) - (2.4) results in:

$$v^{+}(t) = \frac{\Delta v_{dc} + Z_c \Delta i_{dc}}{2} \qquad (2.5)$$

$$v^{-}(t) = \frac{\Delta v_{dc} - Z_c \Delta i_{dc}}{2} \qquad (2.6)$$

$$i^{+}(t) = \frac{\Delta v_{dc} + Z_c \Delta i_{dc}}{2Z_c} \qquad (2.7)$$

$$i^{-}(t) = -\frac{\Delta v_{dc} - Z_c \Delta i_{dc}}{2Z_c} \qquad (2.8)$$

3.0 The protection principle

The fundamental principle of the proposed protection technique presented in this paper is based on Equations (2.5) – (2.8).

3.1 Conditions for forward and reverse fault

For a forward directional fault, the ratio of v^{+} and v^{-} or i^{+} and i^{-} is less than unity; whereas this ratio is greater that unity for reverse directional fault. The principle is explained below.

Considering Figure 3.1, (the inductor located at the cable ends are representative of the inductive effect of HVDC breaker) [3][4]. When the *BTW* arrives at bus A (Figure 3.1), the *FTW* will be generated due to the reflection coefficient at the bus where the surge impedance is discontinuous. In the case of F_1 and with respect to R_{12},

$$v^{+}_{A} = K_A * v^{-}_{A,} \qquad (3.1)$$

Where K_A is reflection coefficient. ($K_A < 1$)

Therefore, $v^{+}_{A} < v^{-}_{A}$ for all internal fault.

Generally, part of the travelling wave components will refracted at the boundary (not shown in the diagram), however this is not a major concern in this study, as energy balance is always maintained at the boundary.

Fig. 3.1 Forward fault showing forward and backward travelling wave.

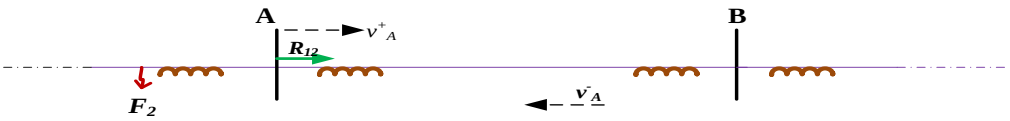

Fig. 3.2, Reverse fault showing forward and backward travelling wave

In Figure 3.2, the first incident wave arriving at relay R_{12} is a *FTW*, and thereafter a *BTW*; following a reflection at terminal B as shown. Therefore in this case,

$$v^+_A > v^-_A$$

From Figures 3.1 and 3.2, for a forward fault, say F_1,

$$v^+_A / v^-_A \ < 1$$

and for a reverse fault say F_2,

$$v^+_A / v^-_A \ > 1$$

3.2 Conditions for forward internal and forward external fault (FIF and FEF)

In Figure 3.3, relay R_{12} sees a much-attenuated *FTW* and *BTW,* due to the discontinuity at the boundary of terminal B.

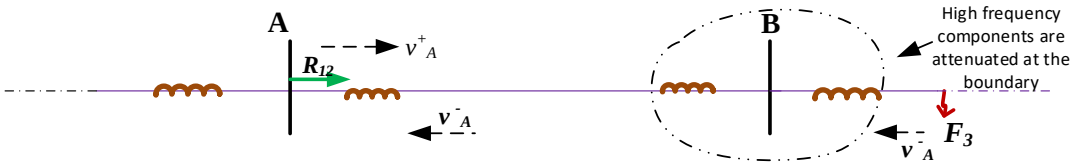

Fig. 3.3 *Travelling wave propagation based on forward external fault (FEF)*

This is largely due to the DC inductor located at each of the line ends, which provides attenuation to the high frequency components resulting from an external fault. However, the attenuation of a travelling wave due to a FIF such as F_1 of Figure 3.1, is much smaller. Therefore the *R-o-C* of the travelling wave components for a FIF would be significantly larger than that for the FEF. This characteristics provides the discriminative criteria between a FIF and a FEF and forms the basis for the protection principle presented in this paper.

It can therefore be said that for a FIF, the magnitude of the *R-o-C* of the forward and backward travelling wave components (voltage and current) must exceed a predetermined setting, otherwise, the fault is a FEF. For the sake of convenience, the following are used in this paper:

dv^+/dt =rate of change (R-o-C) of the forward voltage travelling wave
dv^-/dt =rate of change (R-o-C) of the backward voltage travelling wave
di^+/dt =rate of change (R-o-C) of the forward current travelling wave
di^-/dt =rate of change (R-o-C) of the backward current travelling wave

Therefore the following can be written,

For a FIF,

$$\frac{dv^+}{dt} > \frac{dv^+}{dt}(set)\ ; \qquad \frac{dv^-}{dt} > \frac{dv^-}{dt}(set)$$

$$\frac{di^+}{dt} > \frac{di^+}{dt}(set)\ ; \qquad \frac{di^-}{dt} > \frac{di^-}{dt}(set)$$

For a FEF,

$$\frac{dv^+}{dt} < \frac{dv^+}{dt}(set)\ ; \qquad \frac{dv^-}{dt} < \frac{dv^-}{dt}(set)$$

$$\frac{di^+}{dt} < \frac{di^+}{dt}(set)\ ; \qquad \frac{di^-}{dt} < \frac{di^-}{dt}(set)$$

However, multiplying the derivative of the voltage travelling wave with that of the current travelling wave would significantly improve the sensitivity. The proposed protection algorithm is therefore based on this principle, and it is further explained hereunder.

3.1 Proposed travelling wave-based protection principle

The proposed TWBP principle is based on the magnitude of the product of the magnitude *R-o-C* of the backward voltage and current travelling wave. For an internal fault, the magnitude is significantly greater than a pre-predetermined settings; whereas the magnitude is less than a predetermined setting for forward external faults.

For a FIF,

$$\frac{dv^-}{dt} \times \frac{di^-}{dt} > \frac{dv^-}{dt} \times \frac{di^-}{dt}\ (set)$$

For a FEF,

$$\frac{dv^-}{dt} \times \frac{di^-}{dt} < \frac{dv^-}{dt} \times \frac{di^-}{dt}\ (set)$$

4.0 Simulation studies and validations of the proposed protection algorithm

Simulations were carried out in PSCAD based on a four terminal full-scale DC grid [30] to investigate the proposed TWBP principle for its suitability as a primary protection for DC grid. As shown in Figure 4.1, a DC side inductor has been incorporated to represent the inductive effect of HVDC breaker or fault current limiters or both. These inductors also serve as fault current limiters and provide attenuation for the high frequency components resulting from an external fault.

All fault scenarios indicated were assumed to be a pole-to-ground (P-G) fault, and were applied at *2ms* following the occurrence of the fault; with all measurements taken on the positive pole terminal of the DC link. Generally, faults in DC grids could either be a pole-to-pole (*P-P*) or pole-to-ground (*P-G*), or a double pole-to-ground; however considering the fact that the transmission medium will be based mainly on submarine cables, the P-G faults are more prominent, and therefore forms the basis for the validation of the proposed protection principle. The following critical conditions for the reference relay were assumed. This was a low resistance remote internal faults versus a high resistance external faults. Thus *F1= 300Ω forward internal fault; F2 = 0.01 Ω reverse fault, F3=0.01 Ω forward external fault.*

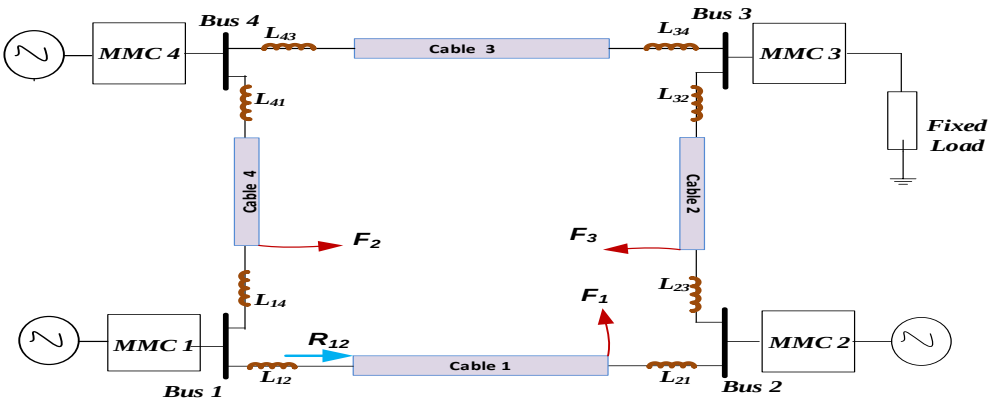

Fig. 4.1 Four terminal DC grid showing critical conditions for relay

(F1= 300Ω forward internal fault; F2 = 0.01 Ω Reverse fault, F3=0.01 Ω forward external)

4.1 Forward and reverse faults

The plots of the voltage and current traveling wave for a forward fault and reverse faults (F_1 and F_2) produced using Equations (2.5) – (2.8) are shown in Figures 4.2 and 4.3 respectively. As shown, during pre-fault conditions, no travelling wave is present; however soon after the occurrence of the fault, travelling waves are developed. In both voltage and current travelling waves of Figure 4.2, the magnitude of the BTW components, v^- and i^- respectively are significantly larger than those of the FTW components, v^+ and i^+ respectively during the first few milliseconds following the application of the fault. This is consistent with the conditions established in Section 3.1 for forward directional faults. The converse is the case for reverse directional fault, F_2 (Figure 4.3), with the magnitude of v^+ and i^+ exceeding those of v^- and i^- during the measurement period. These characteristics provide the discriminative criteria between a forward and reverse fault. Therefore, the ratio between the forward travelling wave component (v^+ or i^+) and the backward travelling wave component (v^- and i^-) provides directional discrimination between a forward and reverse fault.

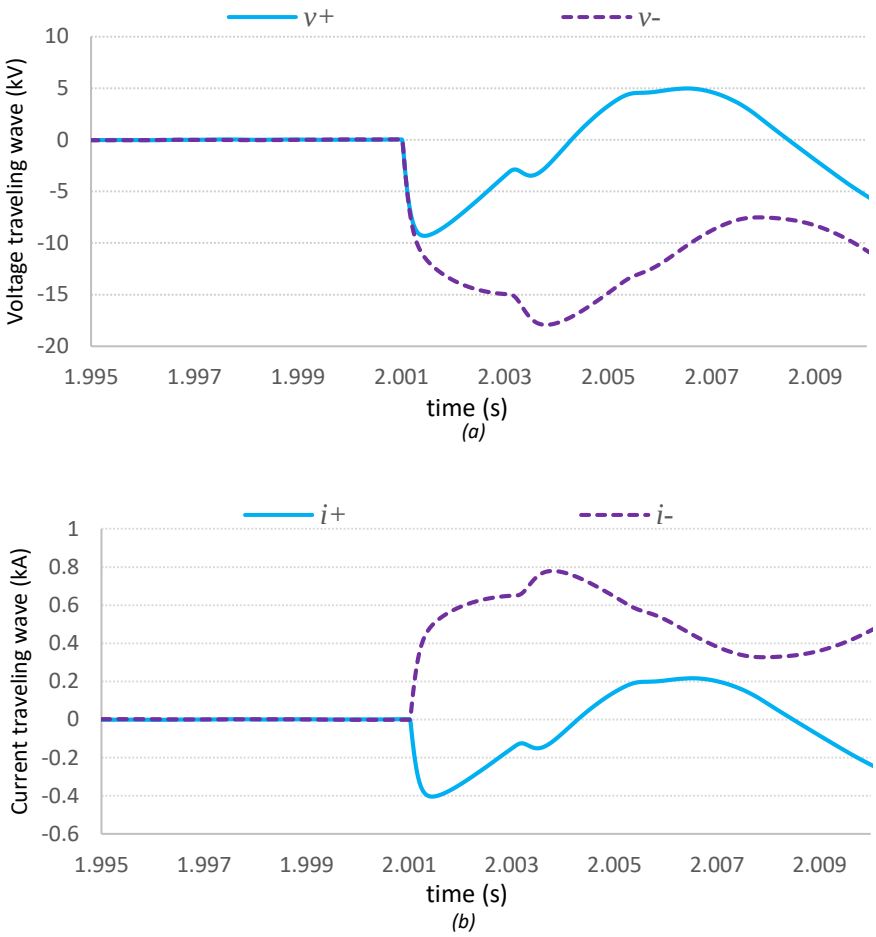

Fig. 4.2 Plots of voltage and current travelling wave for a forward fault (F_1)
(a) Voltage travelling wave (b)Current travelling waves

Thus,

For a forward directional fault,

$$v^+ < v^- \text{ therefore, } v^+/v^- < 1;$$

$$i^+ < i^- \text{ therefore, } i^+/i^- < 1;$$

For a reverse directional fault,

$$v^+ < v^- \text{ therefore, } v^+/v^- > 1;$$

$$i^+ > i^- \text{ therefore, } i^+/i^- > 1;$$

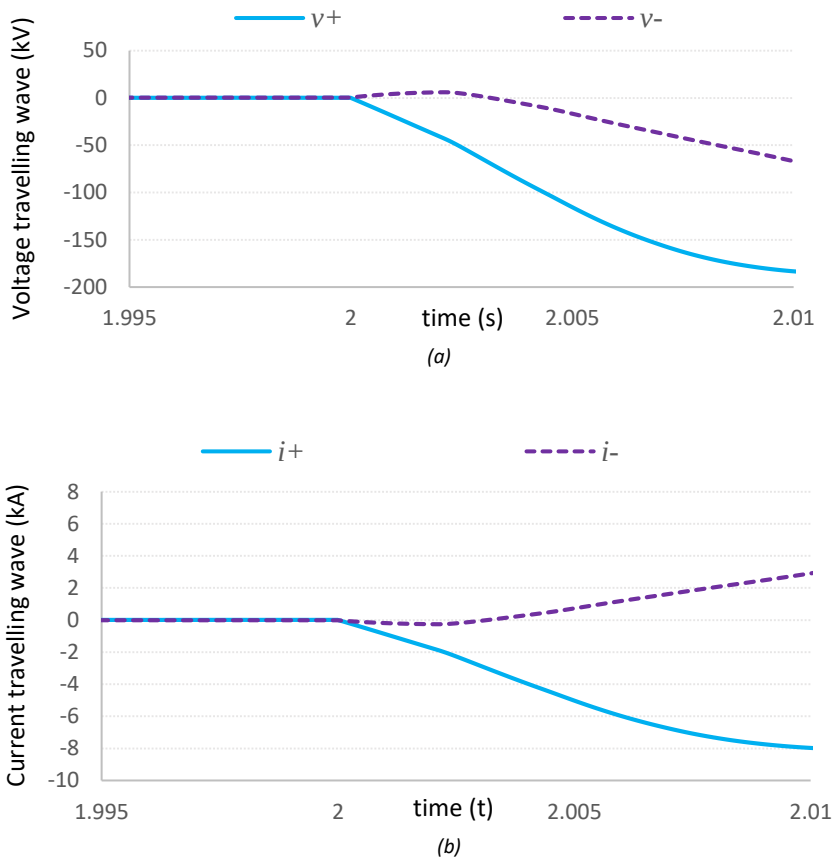

Fig. 4.3 Plots of voltage and current travelling wave for a reverse fault (F_2)
Voltage travelling wave (b)Current travelling waves

However, and for the sake of convenience, this study adopts the ratio of the forward and backward voltage travelling waves for directional discrimination.

4.2 Forward internal versus forward external fault

Figure 4.4 and 4.5 shows the plots of the *R-o-C* of the voltage and current travelling wave for a forward internal and forward external faults with respect to relay R_{12}. As shown, the magnitudes of the *R-o-C* of the travelling wave components for a forward internal faults are significantly larger than those for forward external fault; and hence would provide a good discriminative criterion. This characteristic is also consistent with that established in section 2; and it's largely due to the DC inductors at the boundaries.

Generally, either the forward or backward travelling wave components provide a discriminative criterion between a FIF and FEF. The subscripts "*int*" and "*ext*" represents internal and external faults respectively.

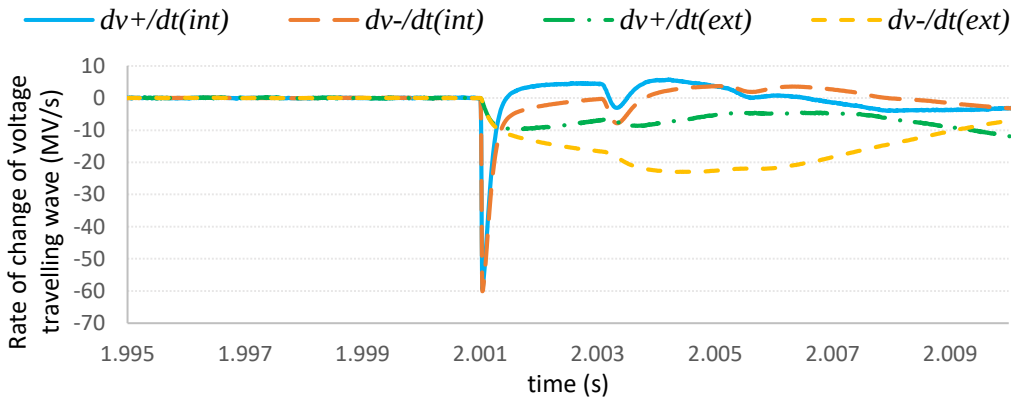

Fig. 4.4 Rate of change (*R-o-C*) of voltage travelling wave for internal and external fault

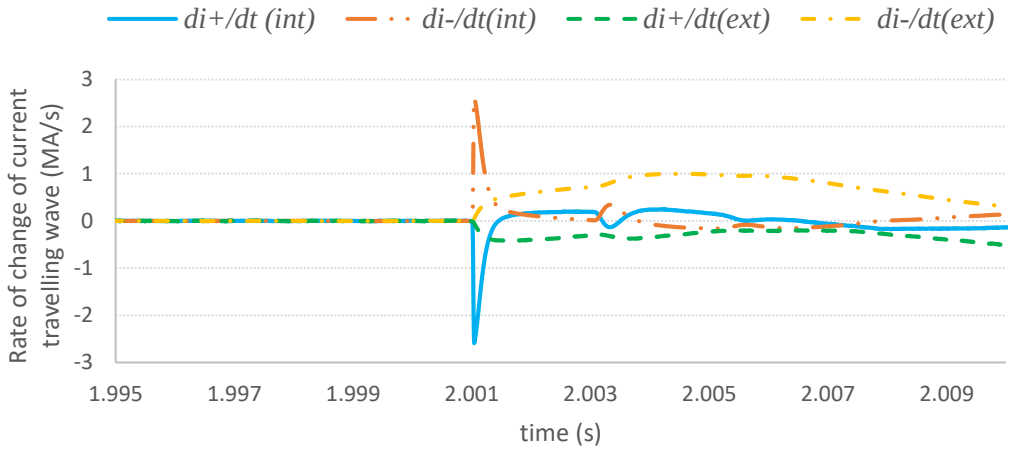

Fig. 4.5 Rate of change (*R-o-C*) of current travelling wave for internal and external fault

However, the plots of Figure 4.6 utilising $\frac{dv^+}{dt} \times \frac{di^+}{dt}$ and $\frac{dv^-}{dt} \times \frac{di^-}{dt}$ indicates an improved sensitivity compared to those of Figures 4.4 and 4.5 utilising $\frac{dv^+}{dt}, \frac{dv^-}{dt}, \frac{di^+}{dt}$ and $\frac{di^-}{dt}$. The calculated results are presented in Table 4.1.

In this paper, the sensitivity of the proposed technique was arrived at by considering the ratio of the relay quantity for an internal fault compared to that for internal fault. This is denoted as the sensitivity index, *Si*

$$Sensitivity\ index, S_i = \frac{Magnitude\ of\ relay\ quantity\ \text{ for internal fault}}{Magnitude\ of\ relay\ quantity\ \text{ for external fault}}$$

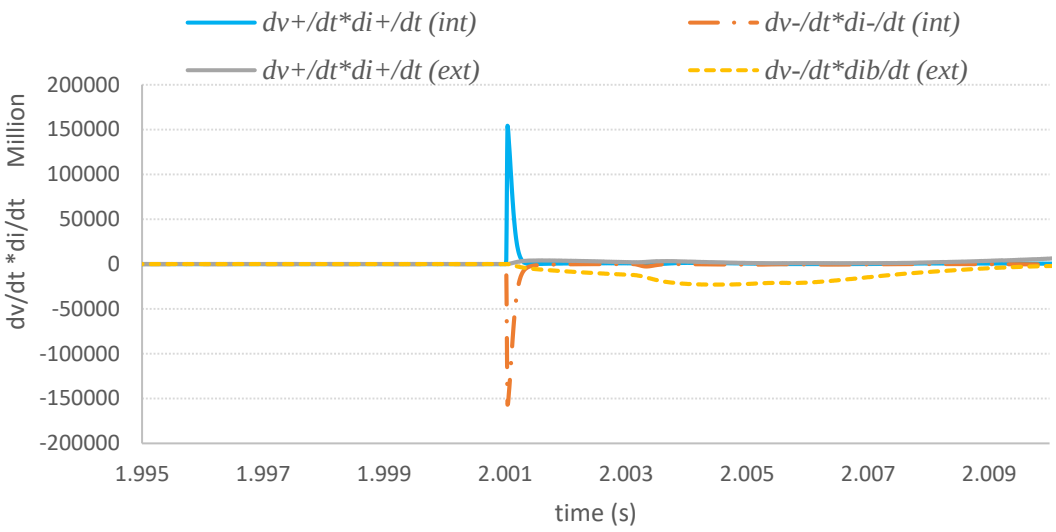

Fig. 4.6 Plots of the product of (*R-o-C*) of voltage and current travelling wave

Table 4.1 Calculated magnitude of the travelling wave quantities for internal and external

Quantity	***Internal fault***	***External fault***	***Sensitivity Indices***
dv^+/dt	*59620*	*10512*	*4.67*
dv^-/dt	*60072*	*10864*	*5.53*
di^+/dt	*2551*	*412*	*5.19*
di^-/dt	*2490*	*445*	*5.60*
$dv^+/dt * di^+/dt$	*149686200*	*3502723*	*41.7*
$dv^-/dt * di^-/dt$	*156902473*	*3649149*	*43.0*

Table 4.1 indicates a higher sensitivity index obtained utilising the product of the magnitude of the R-o-C of the forward and backward travelling wave components ($\frac{dv^+}{dt} \times \frac{di^+}{dt}$ and $\frac{dv^-}{dt} \times \frac{di^-}{dt}$ respectively). However, the magnitude $\frac{dv^-}{dt} \times \frac{di^-}{dt}$ presents the highest sensitivity index, Si. Generally, a higher sensitivity index indicates a better relay performance, which ultimately results in an improved network security. Based on this, the proposed protection principle in this paper utilises the magnitude of $\frac{dv^-}{dt} \times \frac{di^-}{dt}$

4.3 The Protection scheme

The proposed protection strategy adopted in this study utilises the magnitude of the product of the *R-o-C* of the backward travelling wave components ($\frac{dv^-}{dt} \times \frac{di^-}{dt}$) for fault

discrimination. The complete protection scheme is shown in Figure 4.7. As shown, following PSCAD simulations, the resulting data which are representative of the DC voltages and currents recorded at the relay terminals are extracted for post processing. (Figure 4.8).

As shown in Figure 4.7, following the detection of the transient, the travelling wave components are computed using Equations (2.5) – (2.8). Thereafter, the directional comparison unit checks whether the fault is a forward directional or reverse directional fault as explained in section 3.1. Once a forward directional fault is declared, the internal fault detection units computes the *R-o-C* of the travelling wave components. A forward internal fault is declared once the product of the *R-o-C* of the reverse current and voltage travelling wave components exceeds a predetermined setting. The window length was taken as 0.5ms; therefore the decision of whether or not to declare an internal fault is taken during this time frame following the occurrence of fault.

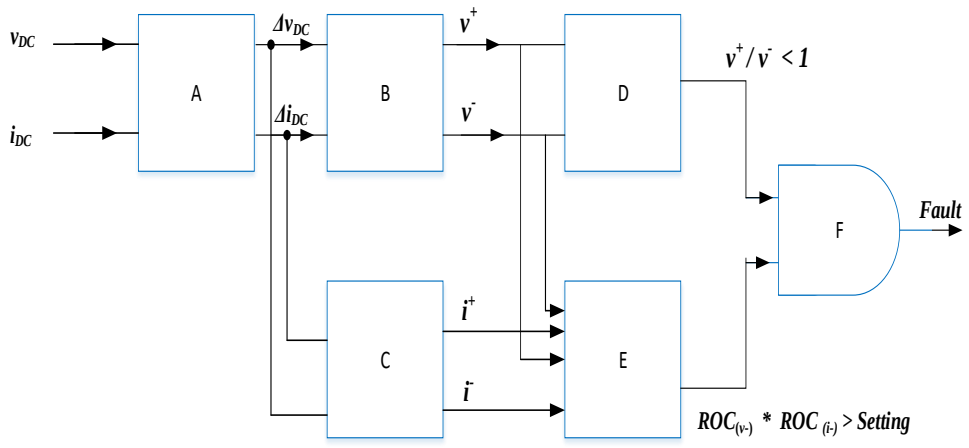

Fig. 4.7 Block diagram of the proposed protection scheme

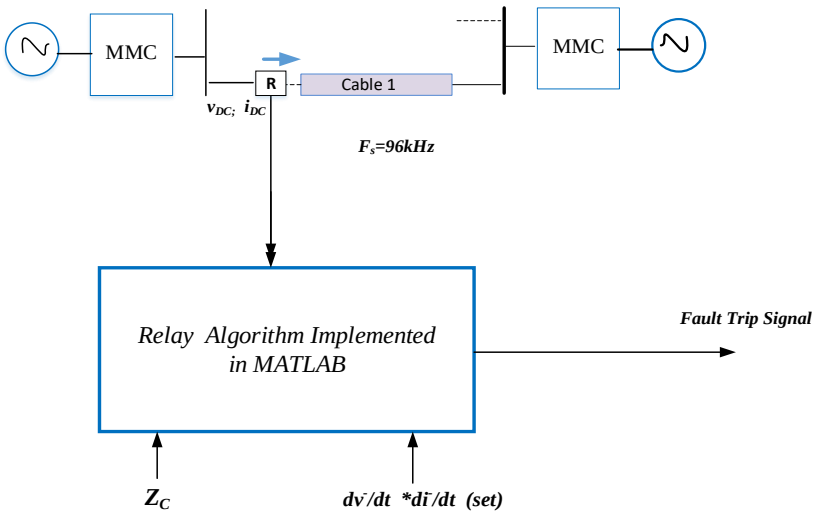

Fig. 4.8 Schematic diagram of the protection scheme

The protection logic is given as

$$If \quad \frac{dv^-}{dt} \times \frac{di^-}{dt} > \frac{dv^-}{dt} \times \frac{di^-}{dt}_{(Set)};$$

Relay operates

Else

Relay remains stable

5.0 Sensitivity analysis

To investigate the sensitivity of the protection scheme, the relay response with respect to a 500Ω fault resistance was investigated. This was assumed to be the most critical condition for the relay. As shown in Figure 4.9, the magnitude of $\frac{dv^-}{dt} \times \frac{di^-}{dt}$ for FIF for a 500Ω fault resistance is significantly larger than that of the FEF with a fault resistance of 0.01 Ω, hence the relay will operate for all internal faults.

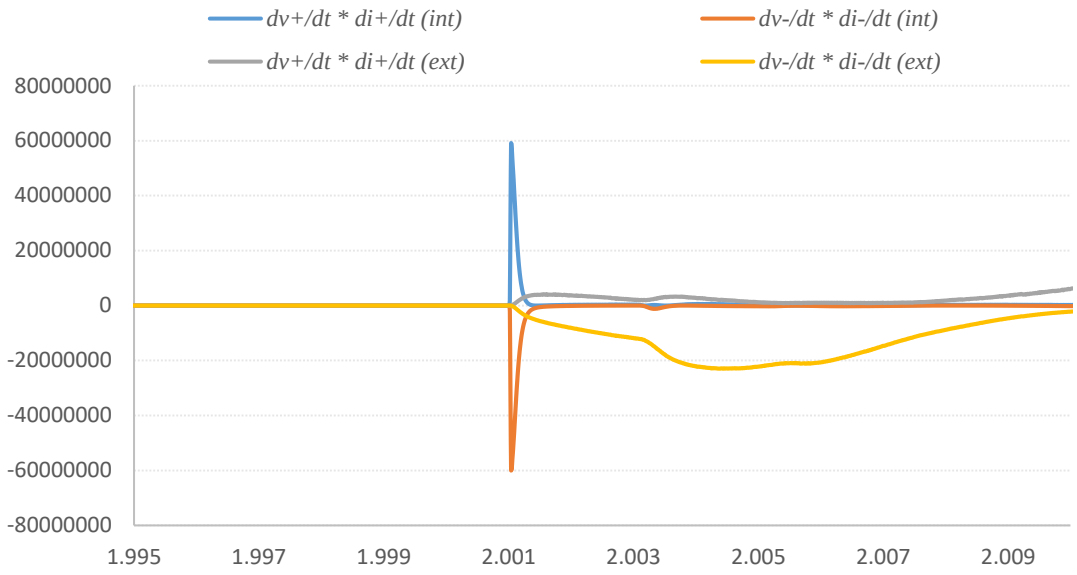

Fig. 4.9 Sensitivity analysis considering *500*Ω fault resistance internal fault versus *0.01* Ω external fault

The sensitivity of the protection scheme was also investigated against proposed protection techniques available in literature. These are the *R-o-C* of the DC current and voltage (the current derivative, $\frac{di_{DC}}{dt}$ and voltage derivative, $\frac{dV_{DC}}{dt}$ respectively). These are shown in Figures 4.10 and 4.11 respectively.

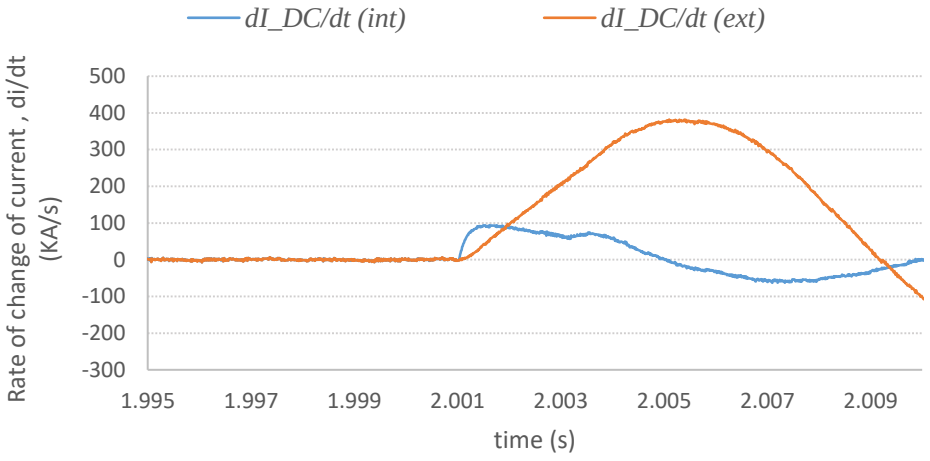

Fig. 4.10 Calculate *R-o-C* of DC current following the inception of fault

As shown in Figure 4.10, for say after *1ms* following fault inception, the $\frac{di_{DC}}{dt}$ for low resistance external fault is significantly larger than that for high resistance internal fault. This is an undesirable condition for the relay and must be avoided to prevent

spurious trips during relay operations. Therefore, the integrity of the $\frac{di_{DC}}{dt}$ technique for DC grid applications is largely dependent on how quickly the initial $\frac{di_{DC}}{dt}$ is measured following the application of fault. Although the sensitivity of the $\frac{dV_{DC}}{dt}$ (Figure 4.11) is improved compared to the $\frac{di_{DC}}{dt}$; a much high sensitivity is obtained by adopting the proposed protection technique ($\frac{dv^{-}}{dt} \times \frac{di^{-}}{dt}$). These are evident in the performance indices shown in Table 4.2 and Figure 4.12 respectively. The values shown are the maximum value of the *R-o-C* of the measured quantity during the first *500µs* following the application of the fault?

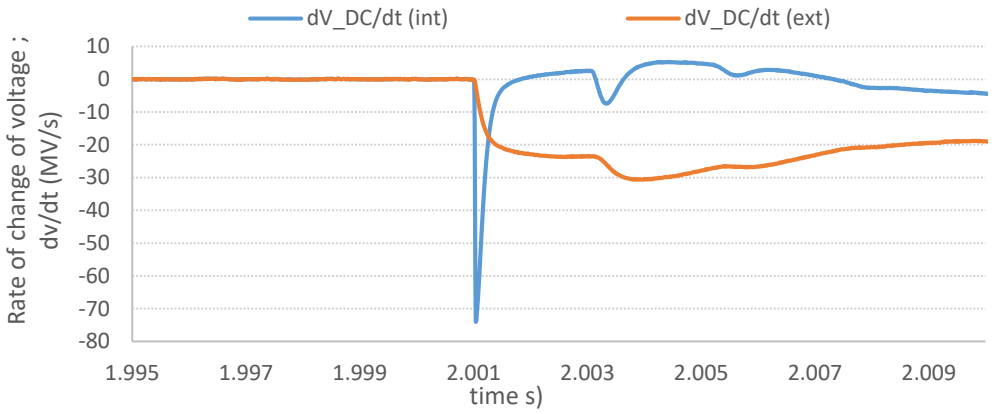

Fig. 4.11 Calculate *R-o-C* of DC voltage following the inception of fault

Table 4.2 Relay Performance Indices for different protection principle.

Product of the RoC of forward travelling wave components	$dv^{-}/dt * di^{-}/dt$	*Internal fault*	*60000000*
		External fault	*2530000*
		Sensitivity index (Si)(Si)	*23.7*
Product of the RoC of backward travelling wave components	$dv^{+}/dt * di^{+}/dt$	*Internal fault*	*60032249*
		External fault	*4293156*
		Sensitivity index (Si)	*13.98*
DC Voltage derivative technique	$dv_{\_DC}/dt$	*Internal fault*	*74039*
		External fault	*13595*
		Sensitivity index (Si)	*5.45*
DC Current derivative technique	$di_{\_DC}/dt$	*Internal fault*	*62*
		External fault	*41*
		Sensitivity index (Si)	*1.51*

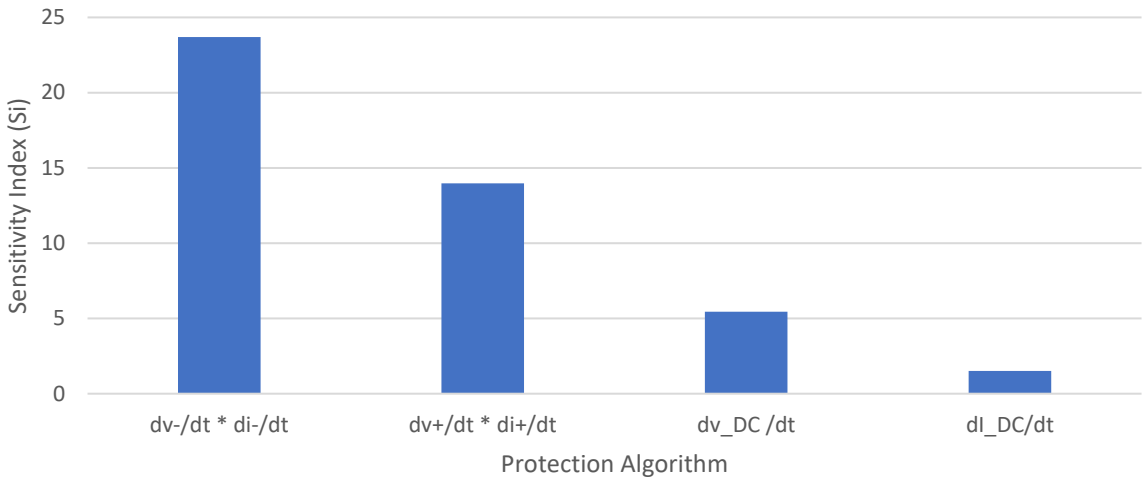

Fig. 4.12 Magnitude of sensitivity index (Si) for proposed and existing protection techniques

Clearly from Figure 4.12, the use of $\frac{dv^-}{dt} \times \frac{di^-}{dt}$ presents the highest sensitivity index compare to other techniques, such as the $\frac{di_{DC}}{dt}$ and $\frac{dV_{DC}}{dt}$.

5.1 Determination of relay setting, computational requirements and speed of the proposed TWBP principle

In this study, the magnitude of $\frac{dv^-}{dt} \times \frac{di^-}{dt}$ for a high resistance remote internal fault for a high resistance fault was taken as the threshold for an internal fault since this scenario gives the most critical condition for the relay. This was theoretically taken as 6×10^7 and it corresponds to the $\frac{dv^-}{dt} \times \frac{di^-}{dt}$ for a 500Ω long distance remote internal fault. However, the practically application is still largely dependent on the availability of commercially available relay having the ability to sample as $96kHz$ or more as well as the speed of the current and voltage transducers.

With an assumed measurement time window of $0.5ms$, this corresponds to 48 samples of the measured travelling wave components. In this study, the arrival time of the travelling wave at the relay terminal (R_{12}) for FIF and FEF are 2.00102s and 2.00112s respectively. Although the fault occur at 2s, however a significant amount of time is required for the travelling wave to arrive to arrive at the relay terminal. Generally, this does not matter because the arrival time of the travelling wave at the relay terminal is

assumed to be t_o; whereas the decision of whether or not to declare an internal fault is made at t_d.

$$t_w = t_d - t_o$$

$$t_w = \text{window length} = 0.5ms$$

The results presented shows that this was achieved during this time frame, and as such is acceptable for DC grid protection. Generally, the operating speed of the HVDC breaker as well as the capability of the current and voltage transducers also has significant effects on the overall performance of the protection algorithm.

6.0 Conclusions

A transient based protection technique utilising the *R-o-C* of the fault induced travelling wave components is presented. The simulation results presented shows the suitability of the proposed protection scheme in discriminating between internal and external fault. The DC inductors located at the cable ends provide attenuation for the high frequency components of the transient signal resulting from an external fault. Generally, large inductors would results in higher sensitivity, however, the choice for this would be a matter of compromise since increasing the size of the inductor will results in increased cost. The results obtained demostrated the reliability and effectivenetss of the protection algorithm. The presented results also revealed that the main fault characteristics are embedded and dominant in the travelling wave components. This is evident in the sensitivity analysis presented in the paper. From the results presented, the proposed protection scheme satisfies the requirement of selectrivity, stability, sensitivity, speed of operation and reliabilty as per protection requirement for future DC grid. Although the protection algorithms were formulated based on lossless cable parameters, the results presented based on validation against a frequency dependent full-scale DC grid models shows the suitability. Key advantages of the proposed algorithms includes the non-reliance on communication, better speed of operation and its simplicity in terms of computational burden and from implementation stand point.

Although, the discriminative criteria between a forward internal fault and a forward external fault is largely due to the bus bar and DC inductors. However, as the trend in

HVDC breakers continue to develop, the need for a protection algorithm without reliance on the DC link inductor is therefore pre-eminent. This brings opportunities for further research in DC grid protection.

References

[1]D. V. Hertem, M. Ghandhari, Multi-terminal VSC HVDC for the European super grid: Obstacles; Renewable and Sustainable Energy Reviews, 14 (2010), 3156-3163

[2]C.D. Barker, R. S. Whitehouse, An Alternative Approach to HVDC Grid Protection, 10th IET Int. Conf. (ACDC2012), Birmingham, May 2012, pp. 1–6

[3]J. Sneath, A.D. Rajapakse, Fault Detection and Interruption in an Earthed HVDC Grid using ROCOV and Hybrid DC Breakers, IEEE Trans. Power Delivery, 31 (2016), pp. 973-981

[4]Wang, J., Berggren, B., Linden, K., et al.: 'Multi-terminal DC system line protection requirement and high speed protection solutions'. CIGRE, Lund, Sweden, 2015, pp. 1–9

[5]S. Azizi, M. Sanaye-Pasand, M. Abedini, A. Hasani, A Traveling-Wave-Based Methodology for Wide-Area Fault Location in Multiterminal DC Systems, IEEE Transactions on Power Delivery, vol. 29 (6) December 2014

[6]Li Yan, Yanfeng Gong, and Bin Jiang. "A novel traveling-wave-based directional protection scheme for MTDC grid with inductive DC terminal", Electric Power Systems Research 157 (2018): 83-92

[7]M. Kong, X. Pei, H. Pang, J. Yang, X. Dong, Y. Wu, X. Zhou, A lifting wavelet-based protection strategy against DC line faults for Zhangbei HVDC Grid in China, 19th European Conference on Power Electronics and Applications (EPE'17 ECCE Europe)

[8]M. Ikhide, S. Tennakoon, A. Griffiths, S. Subramanian, H. Ha, A transient based protection technique for future DC grids utilising travelling wave power, IET Conferences (DPSP), Belfast, UK pp1-6,2018.

[9]L. Jiang, Q. Chen, W. Huang, L. Wang, Y. Zeng, P. Zhao, Pilot Protection Based on Amplitude of Directional Travelling Wave for Voltage Source Converter-High Voltage Direct Current (VSC-HVDC) Transmission Lines, *Energies* 2018, *11*(8), 2021; https://doi.org/10.3390/en11082021

[10]K. Liu, X. Yang, Y. Li, J. Wang; Study of protection for serial multi-terminal DC grids, Journal of International Council on Electrical Engineering, 8:1, 71-77, 2018. DOI: 10.1080/22348972.2018.1466560

[11]K. A. Saleh ; A. Hooshyar ; E. F. El-Saadany, Ultra-High-Speed Travelling-Wave-Based Protection Scheme for Medium-Voltage DC Micro grids, IEEE Transactions on Smart Grid, 2017, 10.1109/TSG.2017.2767552.

[12]Kai Liu ; Youyi Li ; Jianping Wang ; Xiaobo Yang Pilot polarity comparison protection for serial multi-terminals DC grid, IEEE PES Asia-Pacific Power and Energy Engineering Conference (APPEEC), China, 2016

[13] X. Dong, J. Wang, S. Shi, B. Wang, B. Dominik, and M. Redefern, "Traveling Wave Based Single-Phase-to-Ground Protection Method for Power Distribution System," *CSEE J. Power Energy Syst.*, vol. 1, no. 2, pp. 75–82, 2015.

[14] X. Z. Dong, M. A. Redfern, Z. Bo, and F. Jiang, "The application of the wavelet transform of travelling wave phenomena for transient based protection," *Int. Conf. Power Syst. Transients - IPST, New Orleans, USA*, vol. 4, no. 1, pp. 1–6, 2003.

[15]C. Christopoulos., D.W.P. Thomas., A. Wright. "Scheme, based on travelling-waves, for the protection of major transmission lines", *IEE Proceedings,* Vol. 135 (1), pp 63-73, 1998

[16]A. T. Johns, "New ultra-high-speed directional comparison technique for the protection of EHV transmission lines," *Gener. Transm. Distrib. IEE Proc. C*, vol. 127, no. 4, pp. 228–239, 1980.

[17]P.A. Crossley, P.G. McLaren, 'Travelling wave based distance protection', IEEE Trans. Power Appl. Syst. 1983, PAS-102, (9), pp. 2971–298

[18]E. H. Shehab-Eldin and P. G. McLaren, "Travelling wave distance protection-problem areas and solutions," *IEEE Trans. Power Deliv.*, vol. 3, no. 3, pp. 894–902, 1988.

[19]M Chamia, S. Liberman, " Ultra High Speed Relay for EHV/UHV Transmission lines-Development, Design and Applications", IEEE PES Winter Meeting, F78,215-6, Jan./Feb. 1978.

[20]X. Dong, S. Wang, S. Shi, Research on characteristics of voltage fault traveling waves of transmission line, Modern Electric Power Systems, IEEE Conferences, Wroclaw, September 2011.

[21]D. Wang, H. Gao, S. Luo, G. Zou, Ultra-High-Speed Travelling Wave Protection of Transmission Line Using Polarity Comparison Principle Based on Empirical Mode Decomposition, Mathematical Problems in Engineering,
http://dx.doi.org/10.1155/2015/195170

[22]H. Ha, Y. Yang, Y. RuiPeng, Z. Bo, C. Bo, Novel Scheme of Travelling wave based differential protection for bipolar HVDC Transmission Lines, IEEE Conference (POWERCON2010), China, 2010.

[23]B. Zhang, H. Ha, J. Duan, Z. Bo, Boundary Protection, A New Concept for Extra High Voltage Transmission Lines --- Part I: IEEE/PES Transmission and Distribution Conference & Exhibition: Asia and Pacific Dalian, China

[24]Z. Ying Z, T. Nengling, X. Bin, Fault Analysis and Traveling-Wave Protection Scheme for Bipolar HVDC Lines, IEEE Transactions on Power Delivery, 27(2012), pp 1-6

[25]L. Xiaolei, A.H. Osman, O. P. Malik, Hybrid Traveling Wave/Boundary Protection for Monopolar HVDC Line', IEEE Transactions on Power Delivery, Vol. 24, No. 2, April 2009

[26]W. Hao, S. Mirsaeide, X. Kang, X. Dong, D. Tzelepis, A novel travelling wave – based protection scheme for LCC-HVDC systems using Teager Energy Operator, Electric Power and Energy Systems 99 (2018) 474-480

[27] D. Naidoo and N. M. Ijumba, "A protection system for long HVDC transmission lines," *2005 IEEE Power Eng. Soc. Inaug. Conf. Expo. Africa*, pp. 150–155, 2005

[28]C. C. Davidson; R. S. Whitehouse; C. D. Barker; J. P. Dupraz; W. Grieshaber "A new ultra-fast HVDC Circuit breaker for meshed DC networks, 11th IET Int. Conference (ACDC),pp 1-7, 2015.

[29]M. Callavik and A. Blomberg, "The Hybrid HVDC Breaker: An innovation breakthrough enabling reliable HVDC grids," 2012

[30]Manitoba HVDC Research', Four Terminal DC test Grid, 2014, *https://hvdc.ca/*

Appendix

Table A.1.1 Converter and AC side Parameters [30]

Item	Ratings
Rated Power of Converter	800MVA
Rated DC Voltage of Converter	400kV
Converter arm inductance	29mH
Cell DC Capacitor	10000μF
Nominal Frequency	50Hz
Transformer nominal voltage $_{(L-L)\ RMS}$	380kV
Nominal voltage at VSC side $_{(L-L)\ RMS}$	220kV
Leakage reactance of transformer	0.18pu
Rated real power per phase of Load	33MW
Rated reactive power per phase of Load	0.0MW
Rated load voltage$_{(L-G)\ RMS}$	83.72kV

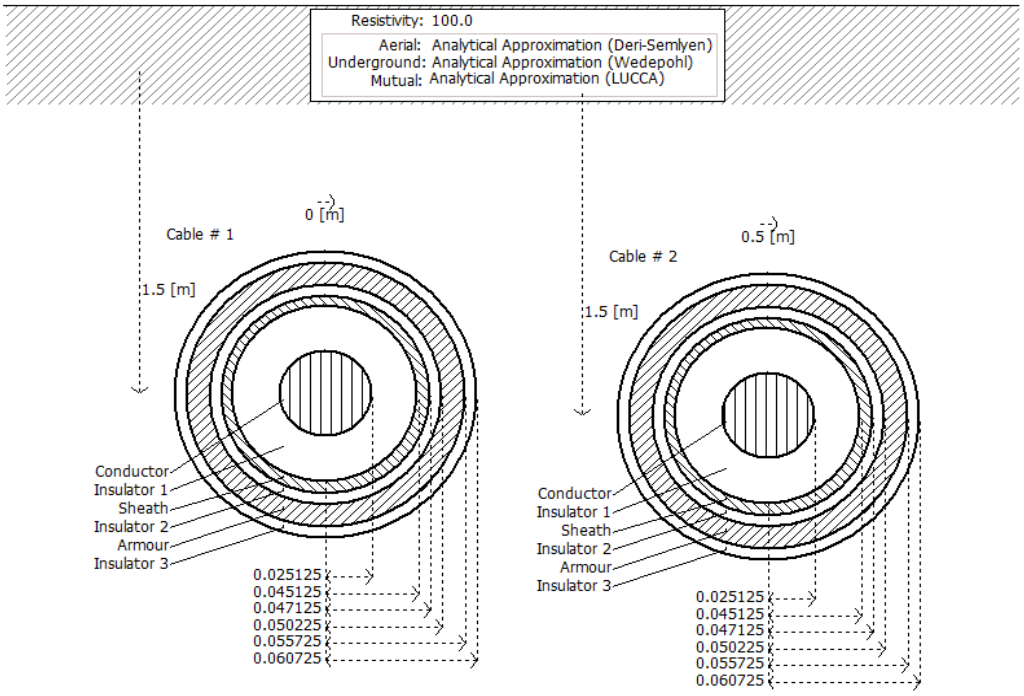

Fig. A1.1 Cable configuration of the HVDC grid [30]

Table A 1.2 Conductor and Insulation Parameters [30]

Item	*Ratings*
Resistivity of core conductor	2.2×10^{-8} Ωm
Resistivity of 1st conducting layer (sheath)	27.4×10^{-8} Ωm
Resistivity of 2nd conducting layer	18.15×10^{-8} Ωm
Outer radius of core conductor	2.51×10^{-2} m
Thickness of 1st conducting layer	2×10^{-3} m
Thickness of 2nd conducting layer	5.5×10^{-3} m
Thickness of 1st insulation layer	2×10^{-2} m
Thickness of 2nd insulation layer	3.1×10^{-3} m
Thickness of 3rd insulation layer	5×10^{-3} m
Relative permittivity of all insulation layer	2.3
All relative permeability	1
Ground resistivity	100 Ωm
Length of Cable	200km